NASA Contractor Report 172295

ICASE

NASA-CR-172295
19840009050

SPECTRAL METHODS FOR THE EULER EQUATIONS:
CHEBYSHEV METHODS AND SHOCK-FITTING

M. Y. Hussaini

D. A. Kopriva

M. D. Salas

T. A. Zang

Contract No. NAS1-17070, NAS1-17130
January 1984

INSTITUTE FOR COMPUTER APPLICATIONS IN SCIENCE AND ENGINEERING
NASA Langley Research Center, Hampton, Virginia 23665

Operated by the Universities Space Research Association

National Aeronautics and
Space Administration

Langley Research Center
Hampton, Virginia 23665

SPECTRAL METHODS FOR THE EULER EQUATIONS:

Chebyshev Methods and Shock-Fitting

M. Y. Hussaini

D. A. Kopriva

Institute for Computer Applications in Science and Engineering

NASA Langley Research Center, Hampton, VA 23665

M. D. Salas

T. A. Zang

NASA Langley Research Center, Hampton, VA 23665

Abstract

The Chebyshev spectral collocation method for the Euler gas-dynamic equations is described. It is used with shock fitting to compute several two-dimensional gas-dynamic flows. Examples include a shock/acoustic wave interaction, a shock/vortex interaction, and the classical blunt body problem. With shock fitting, the spectral method has a clear advantage over second order finite differences in that equivalent accuracy can be obtained with far fewer grid points.

Research for the first and second authors supported by the National Aeronautics and Space Administration under NASA Contract Nos. NAS1-17070 and NAS1-17130 while they were in residence at ICASE, NASA Langley Research Center, Hampton, VA 23665.

Nomenclature

a	sound speed
b	vortex softening length
$\overline{c}_j$	constants in discrete Chebyshev transform
(k_x,k_y)	wavevector
k	wavevector magnitude
p	pressure
(r,θ)	physical polar coordinates
r_b	blunt body boundary
r_s	shock front radius
$s(t)$	start-up function for linear waves
t	physical time
t_s	start-up time for linear waves
u	solution to 1-D test problems
$\tilde{u}$	interpolating polynomial
u_j	solution at collocation points
$\hat{u}_n$	discrete Chebyshev coefficient
(u,v)	physical velocities
x_j	collocation points
x_L	computational left boundary
x_s	shock front location
(x,y)	physical Cartesian coordinates
(x_0,y_0)	center of downstream vortex
y_ℓ	periodicity length in y
A	pressure wave amplitude
B, C	coefficient matrices in Euler equations
L	discrete spatial operator
M, N	number of collocation points
M_s	shock Mach number
P	logarithm of pressure
Q	vector of dependent variables in the Euler equations
Q_{pq}	spectral coefficients of Q
$Q^{(1,0)}_{p,q}$	spectral coefficients of Q_x

$Q_{pq}^{(0,1)}$	spectral coefficients of Q_y
R	source term in the Euler equations
R^+, R^-	linearized 1-D Riemann variables
S	entropy (divided by specific heat at constant volume)
T	computational time
(U,V)	contravariant velocity components
(X,Y)	computational coordinates
β	vertical stretching parameter
γ	ratio of specific heats
Δx	mesh size
Δt	time increment
κ	vortex circulation
ρ	density
σ	smoothing function
θ_c	filter cut-off angle
θ_1	incident angle of pressure wave
θ_{max}	angle of computational outflow boundary
τ_n	Chebyshev polynomial of degree n
ψ	streamfunction

I. Introduction

No convincing case has yet emerged for the spectral shock-capturing technique for the Euler equations. Although solutions can be obtained by such a method, their accuracy tends to be quite low. The filtering procedures necessary to control the oscillations arising from the discontinuity in the solution at the shock have the side-effect of reducing the accuracy in the structured regions of the flow. In a previous paper[1] we reported our experience with a spectral shock-capturing method on a periodic, one-dimensional, compressible flow problem. We found the method to be only first-order accurate and certainly no better than finite difference solutions.

In the present paper we propose a straightforward cure for the oscillations that plague spectral shock-capturing methods: resort to spectral shock-fitting methods instead.

II. Spectral Methods for Shock-Fitting

Shock-fitting techniques have been a standard finite difference tool for some 15 years or so. They are suitable for problems in which the general features of the solution (but not the details) are predictable. This approach overcomes the difficulties of shock-induced oscillations for the simple reason that the shock front itself is a computational boundary. While it eliminates the need for computing derivatives across the shock (which is the source of the oscillations), it adds the complexity of requiring an algorithm to determine the shape and motion of the shock. Spectral methods for shock-fitting are a straightforward combination of both standard techniques. They do, however, require the use of Chebyshev polynomials rather than Fourier series in at least one coordinate direction. We begin this section by discussing the fundamentals of Chebyshev spectral methods.

Basic Chebyshev Spectral Concepts

Consider the model problem

$$u_t + u_x = 0 \tag{1}$$

on $-1 \leq x \leq 1$ with initial condition

$$u(x,0) = \sin(2.5\ \pi x) \tag{2}$$

and boundary condition

$$u(-1,t) = \sin\big(2.5\ \pi(-1-t)\big). \tag{3}$$

The expansion functions are the Chebyshev polynomials

$$\tau_n(x) = \cos(n\ \cos^{-1}\ x) \tag{4}$$

and the collocation points are

$$x_j = \cos\ \frac{\pi j}{N} \qquad j=0,1,\cdots,N. \tag{5}$$

Note that

$$\tau_n(x_j) = \cos\ \frac{\pi jn}{N}\ . \tag{6}$$

The discrete Chebyshev coefficients are

$$\hat{u}_n = \frac{2}{N\bar{c}_n} \sum_{j=0}^{N} \bar{c}_j^{-1}\ u_j\ \cos\ \frac{\pi jn}{N}\ , \tag{7}$$

where

$$\bar{c}_n = \begin{cases} 2 & n = 0 \quad \text{or} \quad N \\ 1 & 1 \leq n \leq N-1 \end{cases} . \tag{8}$$

Thus the interpolating function is

$$\tilde{u}(x) = \sum_{n=0}^{N} \hat{u}_n \, \tau_n(x). \tag{9}$$

The analytic derivative of this function is

$$\frac{\partial \tilde{u}}{\partial x} = \sum_{n=0}^{N} \hat{u}_n^{(1)} \, \tau_n(x), \tag{10}$$

where

$$\begin{aligned} \hat{u}_{N+1}^{(1)} &= 0 \\ \hat{u}_{N}^{(1)} &= 0 \\ \bar{c}_n \, \hat{u}_n^{(1)} &= \hat{u}_{n+2}^{(1)} + 2(n+1)\hat{u}_{n+1} \qquad n=N-1,N-2,\cdots,0 \end{aligned} \tag{11}$$

The Chebyshev spectral derivatives at the collocation points are

$$\left.\frac{\partial \tilde{u}}{\partial x}\right|_j = \sum_{n=0}^{N} \hat{u}_n^{(1)} \cos \frac{\pi j n}{N} . \tag{12}$$

Special versions of the Fast Fourier Transform (FFT) may be used for evaluating the sums in Eqs. (7) and (12). The total cost for a Chebyshev spectral derivative is thus $O(N \ln N)$.

The time-stepping scheme for Eq. (1) must use the boundary conditions to update u_N (at $x = -1$) and the approximate derivatives from Eq. (12) to update u_j for $j=0,1,\cdots,N-1$. Note that no special formula is required for the derivative at $j = 0$ (or $x = +1$). Results at $t = 1$ for a Chebyshev spectral method, a Fourier spectral method and a second-order finite difference method are given in Table I. (The temporal discretization errors are negligible in all cases.) For this non-periodic problem Fourier spectral methods are quite inappropriate, but the Chebyshev spectral method is far superior to the finite difference method.

Table I. Maximum Error for a 1-D Dirichlet Problem

N	Chebyshev Spectral	Fourier Spectral	Finite Difference
4	1.49 (0)	1.85 (0)	1.64 (0)
8	6.92 (-1)	1.92 (0)	1.73 (0)
16	1.50 (-4)	2.27 (0)	1.23 (0)
32	3.45 (-11)	2.28 (0)	3.34 (-1)
64	9.55 (-11)	2.27 (0)	8.44 (-2)

The Chebyshev collocation points are the extreme points of $T_N(x)$. Note that they are not evenly distributed in x, but rather are clustered near the endpoints. The smallest mesh size scales as $1/N^2$. While this distribution contributes to the quality of the Chebyshev approximation and permits the use of the FFT in evaluating the series, it also places a severe time-step limitation on explicit methods for evolution equations.

Filtering for Chebyshev Spectral Methods

The same types of filtering operations that were discussed in Ref. 1 for Fourier spectral methods are applicable to Chebyshev spectral methods as well. In the latter case, however, there is as yet no theoretical support for the usefulness of pre-processing or derivative filtering on simple linear problems.

A straightforward filtering procedure is to mimic Eq. (8) of Ref. 1 by setting

$$u_j = \sum_{n=0}^{N} \sigma\left(\frac{n\pi}{N}\right) \hat{u}_n \cos\left(\frac{n\pi j}{N}\right), \tag{13}$$

where $\hat{u}_n$ is given by Eq. (7) and $\sigma(\theta)$ is a standard smoothing function as described in Ref. 1. There are two problems with this approach: boundary conditions and conservation properties. Neither survives under this type of filtering. The lack of conservation in filtering does not appear to be crucial. After all, the shocks are not being captured, and as will be evident below, the computations use the Euler equations in nonconservation form. Any drift in the mean flow properties in the calculations has been minor. The boundary conditions are another matter. They are enforced after every application of filtering.

A Spectral Shock-Fitted Method

A schematic of the type of spectral shock-fitted calculations described below is illustrated in Fig. 1. At time $t = 0$ an infinite, normal shock at $x = 0$ separates a rapidly moving, uniform fluid on the left from the fluid on the right which is in a quiescent state except for some specified fluctuation. The initial conditions are chosen so that in the absence of any

fluctuation the shock moves uniformly in the positive x-direction with a Mach number (relative to the fluid on the right) denoted by M_s. In the presence of fluctuations the shock front will develop ripples. The shape of the shock is described by the function $x_s(y,t)$. The numerical calculations are used to determine the state of the fluid in the region between the shock front and some suitable left boundary $x_L(t)$ and also to determine the motion and shape of the shock front itself.

Figure 1 is taken from a shock/turbulence calculation[2] in which the downstream fluctuation is a plane vorticity wave that is periodic in y with period y_ℓ. Because of the initial value nature of the calculation, the fluid motion behind the shock is not periodic in x, as Fig. 1 makes abundantly clear. The interesting physical domain is given by

$$x_L(t) \leq x \leq x_s(y,t) \tag{14a}$$

$$0 \leq y \leq y_\ell \tag{14b}$$

$$t \geq 0. \tag{14c}$$

The change of variables

$$X = \frac{x - x_L(t)}{x_s(y,t) - x_L(t)} \tag{15a}$$

$$Y = y/y_\ell \tag{15b}$$

$$T = t \tag{15c}$$

produces the computational domain

$$0 \leq X \leq 1$$

$$0 \leq Y \leq 1 \tag{16}$$

$$T \geq 0.$$

The fluid motion is modeled by the two-dimensional Euler equations. In terms of the computational coordinates these are

$$Q_T + B\,Q_X + C\,Q_Y = 0, \tag{17}$$

where $Q = (P,u,v,S)^T$,

$$B = \begin{bmatrix} U & \gamma X_x & \gamma X_y & 0 \\ \frac{a^2}{\gamma} X_x & U & 0 & 0 \\ \frac{a^2}{\gamma} X_y & 0 & U & 0 \\ 0 & 0 & 0 & U \end{bmatrix} \tag{18}$$

and

$$C = \begin{bmatrix} V & \gamma Y_x & \gamma Y_y & 0 \\ \frac{a^2}{\gamma} Y_x & V & 0 & 0 \\ \frac{a^2}{\gamma} Y_y & 0 & V & 0 \\ 0 & 0 & 0 & V \end{bmatrix}. \tag{19}$$

The contravariant velocity components are given by

$$U = X_t + uX_x + vX_y$$

and (20)

$$V = Y_t + uY_x + vY_y.$$

A subscript denotes partial differentiation with respect to the indicated variable. Reference conditions at downstream infinity are used to normalize p and S; u and v are velocity components in the x and y directions, both scaled by the characteristic velocity defined as the square root of the pressure-density ratio at downstream infinity. A value $\gamma = 1.4$ has been used.

Let n denote the time level and Δt the time increment. The time discretization of Eq. (17) is

$$\tilde{Q} = [1 - \Delta t L^n]Q^n \tag{21}$$

$$Q^{n+1} = \frac{1}{2}\left[Q^n + (1 - \Delta t\tilde{L})\tilde{Q}\right], \tag{22}$$

where L denotes the spatial discretization of $B\,\partial_X + C\,\partial_Y$. The solution Q has the Chebyshev - Fourier series expansion

$$Q(X,Y,T) = \sum_{p=0}^{M} \sum_{q=-N/2}^{N/2-1} Q_{pq}(T)\,\tau_p(\xi)e^{2\pi iqY}, \tag{23}$$

where $\xi = 2X-1$. The derivatives Q_X and Q_Y are approximated by

$$Q_X = 2 \sum_{p=0}^{M} \sum_{q=-N/2}^{N/2-1} Q_{pq}^{(1,0)}(T)\tau_p(\xi)e^{2\pi iqY}, \tag{24}$$

$$Q_Y = 2\pi \sum_{p=0}^{M} \sum_{q=-N/2}^{N/2-1} Q_{pq}^{(0,1)}(T)\tau_p(\xi)e^{2\pi iqY} \tag{25}$$

where $Q_{pq}^{(1,0)}$ is computed from Q_{pq} in a manner analogous to Eq. (11) and

$$Q_{pq}^{(0,1)} = i\, q\, Q_{pq}. \tag{26}$$

The most critical part of the calculation is the treatment of the shock front. The shock-fitting approach used here is desirable because it avoids the severe post-shock oscillations that plague shock-capturing methods. The time derivative of the Rankine-Hugoniot relations provides an equation for the shock acceleration. This equation is integrated to update the shock position (see Ref. 3 for details). This method is a generalization of the finite difference method developed by Pao and Salas[4] for their study of the shock/vortex interaction.

Boundary Conditions

The correct boundary conditions at the left boundary depends upon the relative Mach number. For uniform flow and $\gamma = 1.4$ the flow behind the shock is supersonic if $M_s > 2.08$. In this case the boundary at x_L is a supersonic inflow boundary and it is appropriate to specify all variables. If $M_s < 2.08$ then the left boundary is a subsonic inflow boundary. The advisable procedure, then, is to base the numerical boundary conditions on the linearized characteristics of the Euler equations. At the left (subsonic) boundary the (linearized) characteristic variables corresponding to the outgoing characteristic direction are

$$R^- = P - \frac{\gamma}{a} u. \tag{27}$$

Similarly,

$$R^+ = P + \frac{\gamma}{a} u \tag{28}$$

corresponds to the outgoing characteristic direction at the right (subsonic) boundary which is used by the shock fitting algorithm.

A set of successful boundary conditions on the left is obtained by first calculating preliminary values of all quantities at the left boundary and then incorporating the given values of S, v, and R^+ as

$$\begin{aligned} S &= S_{given} \\ v &= v_{given} \\ P + \frac{\gamma}{a} u &= R^+_{given} \\ P - \frac{\gamma}{a} u &= P_{prelim} - \frac{\gamma}{a} u_{prelim} \end{aligned} \tag{29}$$

Thus, the PDE is used to update the appropriate characteristic combination of variables at the boundary. The characteristic analysis is given in Ref. 5. The particular boundary condition was advocated in Ref. 6. For the right boundary a similar characteristic correction procedure can be incorporated into the evaluation of the shock velocity.

The global nature of spectral methods makes them even more sensitive to the boundary conditions than finite difference methods. An illustration of just how unforgiving spectral methods can be is provided in Fig. 2. Shown

there are two spectral shock-fitted calculations of the interaction of a Mach 1.3 shock with a Karman vortex street. (See Ref. 7 for more details about this problem.) The top row shows what happens when all flow variables are specified at the left, subsonic, inflow boundary, whereas the bottom row displays a calculation which is identical except for the use of Eq. (29) as the inflow boundary condition. The former calculation is clearly contaminated by oscillations emanating from the inflow boundary. The latter calculation makes clear that no physical signals have yet reached the inflow location even though in the spectral method numerical signals reach the inflow instantaneously. Finite difference calculations for this same problem were reported in Ref. 7. Despite the fact that an overspecified inflow boundary condition was used, no analogous problem arose because of the local nature of the discretization.

III. Results for Chebyshev Spectral Shock-Fitting

Shock/Turbulence Interaction

The nonlinear interaction of plane waves with shocks was examined at length in Ref. 2. The numerical method used there was similar to the one described above but employed second-order finite differences in place of the present Chebyshev-Fourier spectral discretization. Detailed comparisons were made in Ref. 2 with the predictions of linear theory.[8] The linear results turned out to be surprisingly robust, remaining valid at very low (but still supersonic) Mach numbers and at very high incident wave amplitudes. The only substantial disagreement occurred for incident waves whose wave fronts were nearly perpendicular to the shock front. This type of shock-turbulence interaction is a useful test of the spectral technique because the method can

be calibrated in the regions for which linear theory has been shown to be valid.

The most reliable numerical results can be obtained for the acoustic responses to acoustic waves. Unlike the vorticity responses, these require no differentiation of the flow variables, thus eliminating one extra source of error. Moreover, the acoustic reponse stretches much further behind the shock than the vorticity response, thus providing greater statistical reliability. Vorticity response results are reported in Ref. 9. The incident pressure wave is taken to be

$$p_1' = A_1' \, e^{i(\underline{k}_1 \cdot \underline{x} - \omega_1 t)} \tag{30}$$

where $\underline{k}_1 = (k_{1,x}, k_{1,y})$, $\omega_1 = M_s a_1 \, k_{1,x} + a_1 \, k_1$ and A_1' is the amplitude. In terms of the incidence angle θ_1, $\underline{k}_1 = (k_1 \cos \theta_1, k_1 \sin \theta_1)$. The linearized transmitted acoustic wave can be expressed in the same manner with all subscripts changed from 1 to 2. The amplification coefficient for the transmitted acoustic wave is then the ratio A_2'/A_1'. Figure 3 indicates the transmission coefficient extracted from the computation. At each fixed value of X we perform a Fourier analysis in Y of the pressure. The Fourier coefficient for $q = 1$ provides the amplitude A_2'. In order to reduce the transients that would accompany an abrupt start of the calculation at full wave amplitude, an extra factor of $s(t)$ is inserted into Eq. (30), where

$$s(t) = \begin{cases} 3(t/t_s)^2 - 2(t/t_s)^3 & 0 \leq t \leq t_s \\ 1 & t \geq t_s \end{cases} . \tag{31}$$

The start-up time t_s is some multiple (typically $1/2$) of the time it takes the shock to encounter one full wavelength (in the x-direction) of the

incident wave. The ratio A_2'/A_1' is plotted in Fig. 3 as a function of the mean value of the physical coordinate x corresponding to X. The start-up time for this Mach 3 case is $t_s = 0.56$. The average of the x-dependent responses between the start-up interval and the shock produces the computed transmission coefficient. The standard deviation of the individual responses serves as an error estimate.

The dependence upon incidence angle of the acoustic transmission coefficient for $A_1' = 0.001$, and $M_s = 3$ waves is displayed in Fig. 4. As is discussed in Ref. 2, linear theory is quite reliable at angles below, say, 45^o. Figure 4 contains results from both spectral and finite difference calculations. The finite difference results were obtained with the same second-order MacCormack's method that was described in Ref. 2 except that periodic boundary conditions (rather than stretching) were employed in the y-direction. The finite difference grid was 64 × 16 and these calculations used a CFL number of 0.70. The spectral grid was 32 × 8, the CFL number was 0.50. (No solution smoothing was applied.) Figure 4 shows that both methods produce the same results. A head-to-head comparison of both methods for the $\theta_1 = 10^o$ case is provided in Table II. The "exact" value is taken from linear theory.[8] Since the amplitude of the incident acoustic wave is so small, it should come as no surprise that four points in the y-direction suffice for the spectral calculation. Note that the standard deviations are substantially smaller for the spectral method. These results suggest that the spectral method requires only half as many grid points in each coordinate direction.

Table II. Grid Dependence of Acoustic Transmission Coefficient

Grid	Finite Difference	Chebyshev-Fourier Spectral
16 × 4	6.403 ± 2.652	7.257 ± 0.587
16 × 8	6.427 ± 2.626	7.257 ± 0.587
32 × 4	7.105 ± 0.453	7.158 ± 0.022
32 × 8	7.134 ± 0.471	7.158 ± 0.022
32 × 16	7.139 ± 0.497	7.158 ± 0.022
64 × 16	7.163 ± 0.078	7.157 ± 0.017
128 × 16	7.152 ± 0.022	
"exact"	7.156	7.156

Shock/Vortex Interaction

This problem is closely related to the previous one. The downstream field is not the linear plane pressure wave of Eq. (30) but an idealized vortex in which the density is constant, the velocities are derivable from the stream function

$$\psi = \frac{\kappa}{2\pi} \log \sqrt{b^2 + (x - x_0)^2 + (y - y_0)^2} \ , \tag{32}$$

the pressure from Bernoulli's equation, and the temperature from the equation of state. This model approaches an idealized incompressible point vortex at large distances from the vortex center at (x_0, y_0), but it is much smoother in the core. The specific example provided here has the circulation $\kappa = 0.40$; the vortex softening scale $b = 0.1$ and the vortex is located at $(x_0, y_0) = (0.5, 0.0)$.

Note that periodic boundary conditions in y are no longer appropriate. Accordingly, Eqs. (14b) and (15b) are replaced by

$$-\infty < y < \infty \tag{33a}$$

and

$$Y = \frac{\tanh(\beta y) + 1}{2} , \tag{33b}$$

respectively, where the stretching parameter β is of order one. Moreover, the spectral method now uses Chebyshev series in Y as well as X. The analogs of Eqs. (14) - (26) are given in full in Ref. 7. (Incidentally, it was this Chebyshev - Chebyshev algorithm which was used in the production of Fig. 2.)

The computed results for the shock-vortex interaction at $t = 0.35$ are given in Fig. 5 for both finite difference and spectral methods. The contour levels are the same in the two diagrams. The finite difference calculation used a 75×50 grid whereas the spectral result was obtained with a 32×16 grid, with a CFL number of 0.50 and solution smoothing using the exponential cut-off applied every 80 time-steps. The major difference between the results is that the spectral calculation does not have as deep a pressure minimum as the finite difference result.

Supersonic Flow Past a Circular Cylinder

The classical problem of a blunt body such as a circular cylinder in a supersonic stream has been an ideal test problem for numerical methods since it provides a relatively simple well-posed transonic problem with nontrivial initial and boundary conditions. The present spectral method obtains the steady state solution as the time asymptotic solution of the unsteady Euler

equations which are written in the cylindrical polar coordinate (r,θ) system. The physical domain of interest consists of the known body $r = r_b(\theta)$, the unknown shock location $r = r_s(\theta,t)$, the axis of symmetry (at the front stagnation streamline $\theta = \pi$) and the outflow boundary $\theta = \pi - \theta_{max}$. For the purpose of shock fitting, the coordinate transformation

$$X = \frac{r - r_b(\theta)}{r_s(\theta,t) - r_b(\theta)} \tag{34a}$$

$$Y = \frac{\pi - \theta}{\theta_{max}} \tag{34b}$$

is introduced so that the shock wave and the body are coordinate lines in the transformed domain. The transformed equations of motion, in the notation of the shock interaction problems, are

$$Q_T + B\,Q_X + C\,Q_Y + R = 0, \tag{35}$$

where

$$B = \begin{bmatrix} U & \gamma X_r & (\gamma/r)X_\theta & 0 \\ (a^2/\gamma)X_r & U & 0 & 0 \\ (a^2/\gamma)(1/r)X_\theta & 0 & U & 0 \\ 0 & 0 & 0 & U \end{bmatrix}, \tag{36}$$

$$C = \begin{bmatrix} V & \gamma Y_r & (\gamma/r)Y_\theta & 0 \\ (a^2/\gamma)Y_r & V & 0 & 0 \\ (a^2/\gamma)(1/r)Y_\theta & 0 & V & 0 \\ 0 & 0 & 0 & V \end{bmatrix}, \tag{37}$$

and

$$R = \left[\gamma \frac{u}{r} , - \frac{v^2}{r} , \frac{uv}{r} , 0\right]^T \tag{38}$$

with

$$U = X_t + u X_r + \frac{v}{r} X_\theta$$

$$V = \frac{v}{r} Y_\theta \ . \tag{39}$$

The flow field variables are expanded in double Chebyshev series, and the solution technique is the same as for the previous problem.

The shock boundary $r = r_s(\theta,t)$ (i.e., $X = 1$) is computed using the Rankine-Hugoniot jump conditions and the compatibility equation along the outgoing characteristic from the high pressure side of the shock. On the body $r = r_b(\theta)$ (i.e., $X = 0$), the normal component of velocity u is zero. The limiting angle θ_{max} is chosen so that the outflow boundary $Y = 1$ is supersonic, and hence no boundary conditions need be imposed.

At the symmetry line $\theta = \pi$ (or $Y = 0$) the tangential velocity component v is set to zero. The variables P, S, and u (as well as the shock velocity) satisfy the condition that their derivatives with respect to Y are zero there. This is enforced at each stage of the predictor-corrector time discretization (see Eqs. (21) and (22)) by simply using the value zero and not the standard Chebyshev spectral Y-derivative values for P, S, and u at $Y = 0$.

The filtering employed in the calculations reported below was solution smoothing every 50 time-steps using the quartic taper (Eq. (12) of Ref. 1) with $\theta_c = 2\pi/3$. After each filtering step the boundary conditions were applied: u was set to zero on the body and v to zero on the symmetry line; moreover, the Neumann boundary conditions at $Y = 0$ were enforced by

transforming to wavenumber space, adjusting the very highest Chebyshev coefficient as needed, and then transforming back to physical space.

Several calculations have been performed for the flow of an intially uniform stream past a circular cylinder. The limiting angle θ_{max} was 80^{o}, the collocation grid was 9 × 9, the CFL number was 0.20 and 2000 time-steps were taken. Results for the Mach 4 case are illustrated in Fig. 6. Note that the essential features of the flow are evident even on this very coarse grid. (Indeed, it is the small number of data points which is responsible for the jagged appearance of the contour lines.) Similar results have been obtained for the Mach 2 and Mach 6 situations. Table III presents a comparison of the computed values of the stagnation pressure with the theoretical results.[10] Since the numerical computations have converged to only 3 or 4 digits after 2000 time-steps, the performance of the spectral discretization may be even better than implied by Table III. We re-emphasize the fact that there remains the clear need for effective means of surmounting the severe explicit time-step restriction which besets current Chebyshev spectral methods.

Results for a more challenging flow are shown in Fig. 7. Finite difference results (on a 20 × 30 grid) are given in Fig. 8 for comparison. The linearly-sheared stream produces a recirculating region. The 9 × 9 spectral grid is still capable of resolving this essential feature.

Table III. Comparison of Stagnation Pressures for Uniform Flow Past a Circular Cylinder

Mach Number	Calculated Pressure	Theoretical Pressure	Percent Relative Error
2	5.651	5.6408	0.18
4	21.072	21.0750	-0.014
6	46.846	46.8109	0.075

VI. Conclusions

Our results demonstrate that spectral shock-fitting methods for compressible flows are viable techniques. The quantitative comparison for the shock/acoustic wave problem shows the superior performance of the spectral method. Similar performance is observed on the shock/vortex and blunt body problems when the spectral results are compared with finite difference results obtained on a much finer grid.

Our experience shows that before the full potential of spectral methods is realized several aspects must be improved. First, filtering techniques for both Fourier and Chebyshev methods need to be refined. For filtering in Chebyshev methods the problem of conservation and boundary conditions must be resolved. Finally, for non-periodic problems the collocation grid distribution imposes a severe restriction on the explicit time-stepping used throughout this paper. Implicit time-stepping, on the other hand, involves expensive inversion of full matrices. There is a clear need to develop efficient acceleration techniques.

References

[1]Hussaini, M. Y., Kopriva, D. A., Salas, M. D., and Zang, T. A., "Spectral Methods for the Euler Equations: Fourier Methods and Shock-Capturing," NASA CR-172294, January 1984.

[2]Zang, T. A., Hussaini, M. Y., and Bushnell, D. M., "Numerical Computations of Turbulence Amplification in Shock Wave Interactions," AIAA J., Vol. 22, January 1984, pp. 13-21.

[3]Hussaini, M. Y., Salas, M. D., and Zang, T. A., "Spectral Methods for Inviscid, Compressible Flows," Advances in Computational Transonics, W. G. Habashi, ed., Pineridge Press, Swansea, UK, to appear March 1984.

[4]Pao, S. P. and Salas, M. D., "A Numerical Study of Two-Dimensional Shock Vortex Interaction," AIAA Paper 81-1205, 1981.

[5]Oliger, J. and Sundström, A., "Theoretical and Practical Aspects of Some Initial Boundary Value Problems in Fluid Dynamics," SIAM J. Appl. Math., Vol. 35, November 1978, pp. 419-446.

[6]Gottlieb, D., Gunzburger, M., and Turkel, E., "On Numerical Boundary Treatment of Hyperbolic Systems for Finite Difference and Finite Element Methods," SIAM J. Numer. Anal., Vol. 19, August 1982, pp. 671-682.

[7]Salas, M. D., Zang, T. A., and Hussaini, M. Y., "Shock-fitted Euler Solutions to Shock-Vortex Interactions," Proc. of the 8th Intl. Conf. on Numerical Methods in Fluid Dynamics, E. Krause, ed., Springer-Verlag, 1982.

[8]Ribner, H. S., "Shock-Turbulence Interaction and the Generation of Noise, NACA Report 1233, 1955.

[9]Zang, T. A, Kopriva, D. A. and Hussaini, M. Y., "Pseudospectral Calculation of Shock Turbulence Interactions," Proc. of the 3rd Intl. Conf. on Numerical Methods in Laminar and Turbulent Flow, C. Taylor, ed., Pineridge Press, 1983, pp. 210-220.

[10]Ames Research Staff, "Equations, Tables, and Charts for Compressible Flow", NACA Report 1135, 1953.

Figure Captions

Fig. 1. Typical shock-fitted time dependent flow model in the physical plane.

Fig. 2. Spectral pressure distribution for a Mach 1.3 Karman vortex street showing sensitivity to inflow boundary conditions.

Fig. 3. Post-shock dependence of the pressure response to a pressure wave incident at 10^{o} to a Mach 3 shock. The solid line is the linear theory prediction. The circles are the spectral solution.

Fig. 4. Dependence on incident angle of the pressure response to a 0.1% amplitude pressure wave incident on a Mach 3 shock. The solid line is the linear theory result. Circles are spectral solutions, squares are finite difference solutions.

Fig. 5. Pressure contours for spectral (SP) and finite difference (FD) calculations of the shock/vortex interaction problem. The spectral solution used a 32×16 grid and the finite difference used a 75×50 grid.

Fig. 6. Spectral solution on a 9×9 grid for a circular cylinder in a Mach 4 uniform stream.

Fig. 7. Spectral solution on a 9×9 grid for a circular cylinder in a linearly sheared stream.

Fig. 8. Finite difference solution on a 20×30 grid for a circular cylinder in a linearly sheared stream.

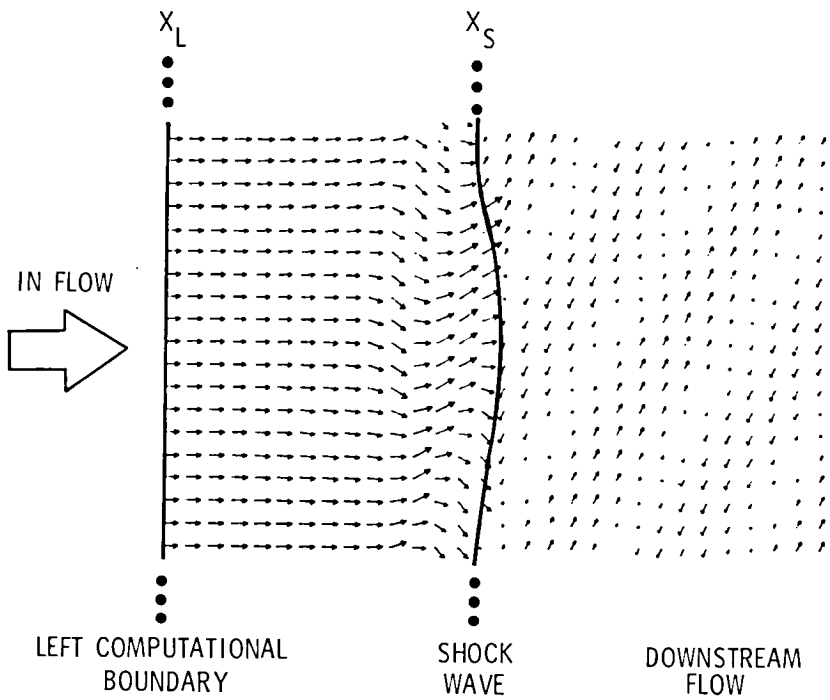
X_L
X_S
IN FLOW
LEFT COMPUTATIONAL BOUNDARY
SHOCK WAVE
DOWNSTREAM FLOW

Figure 1

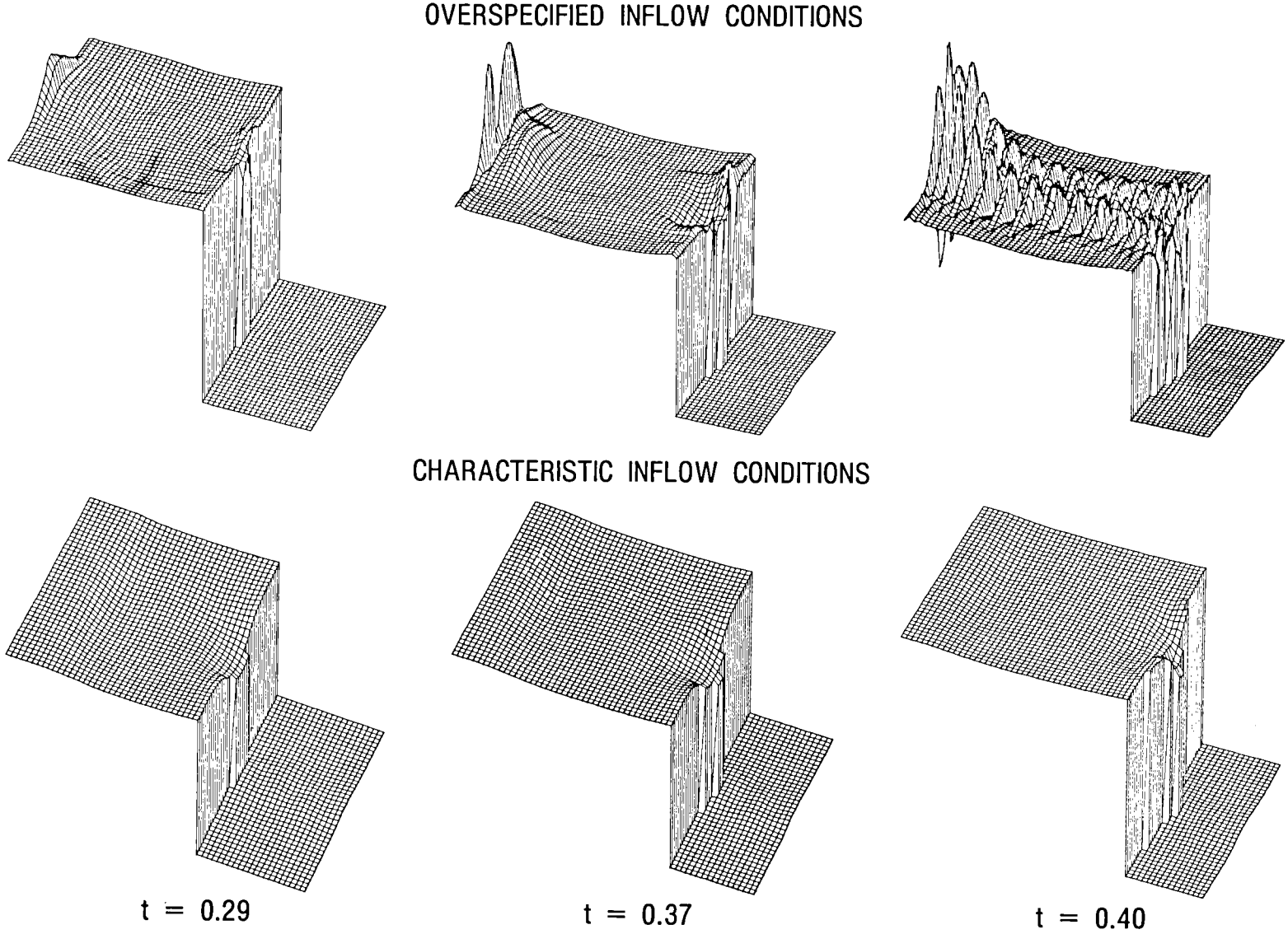
OVERSPECIFIED INFLOW CONDITIONS
CHARACTERISTIC INFLOW CONDITIONS
t = 0.29
t = 0.37
t = 0.40

Figure 2

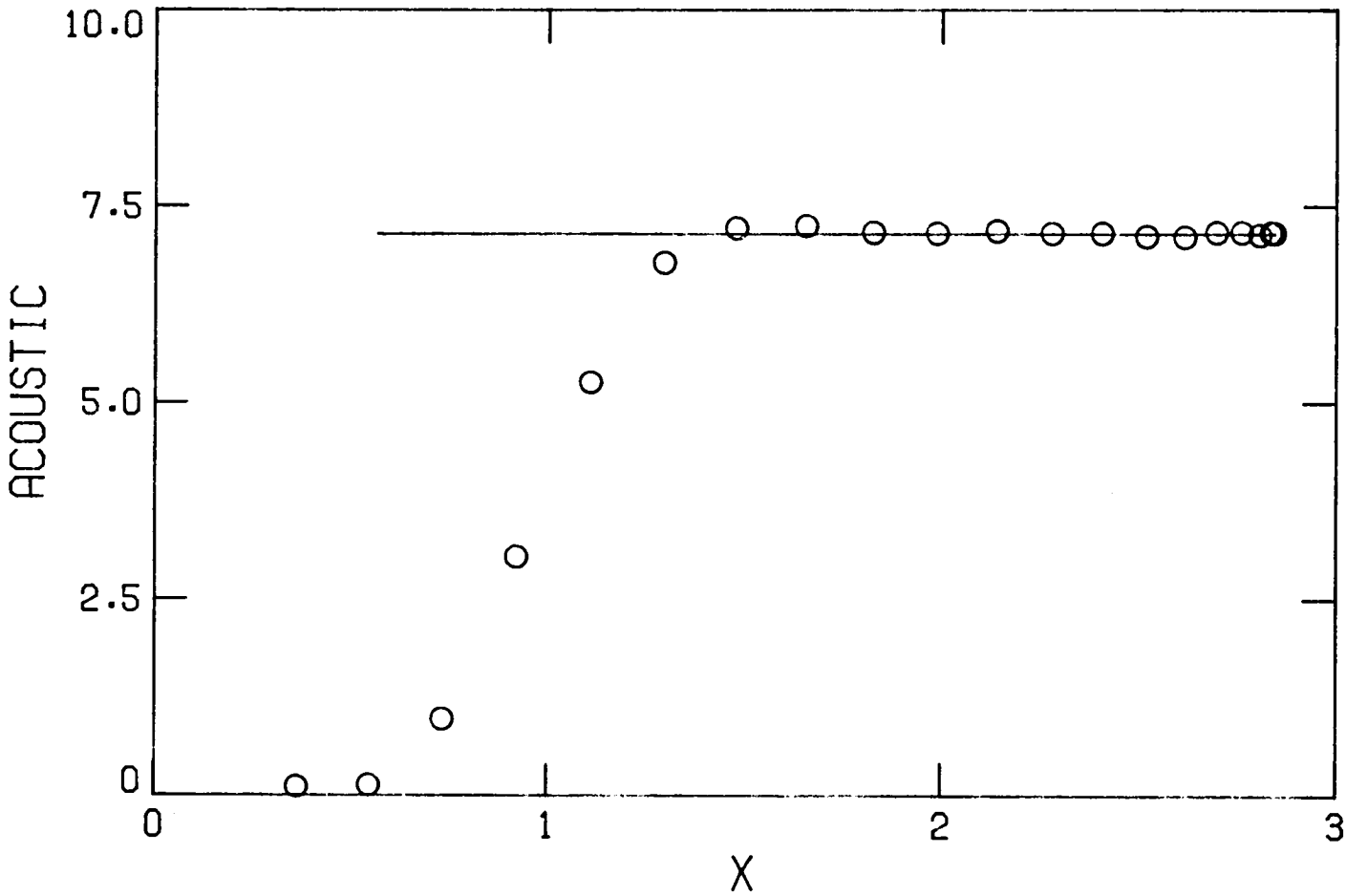

Figure 3

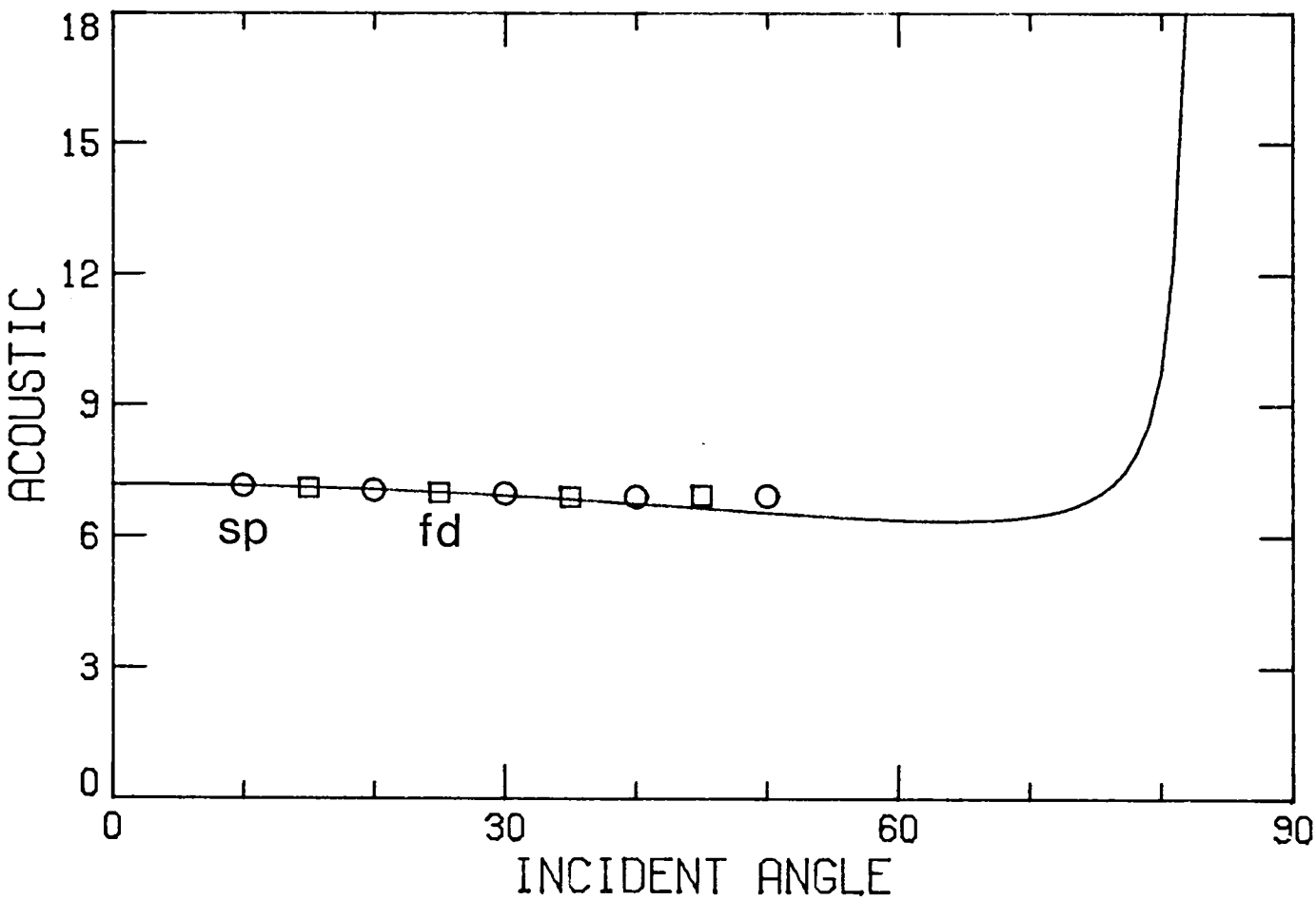

Figure 4

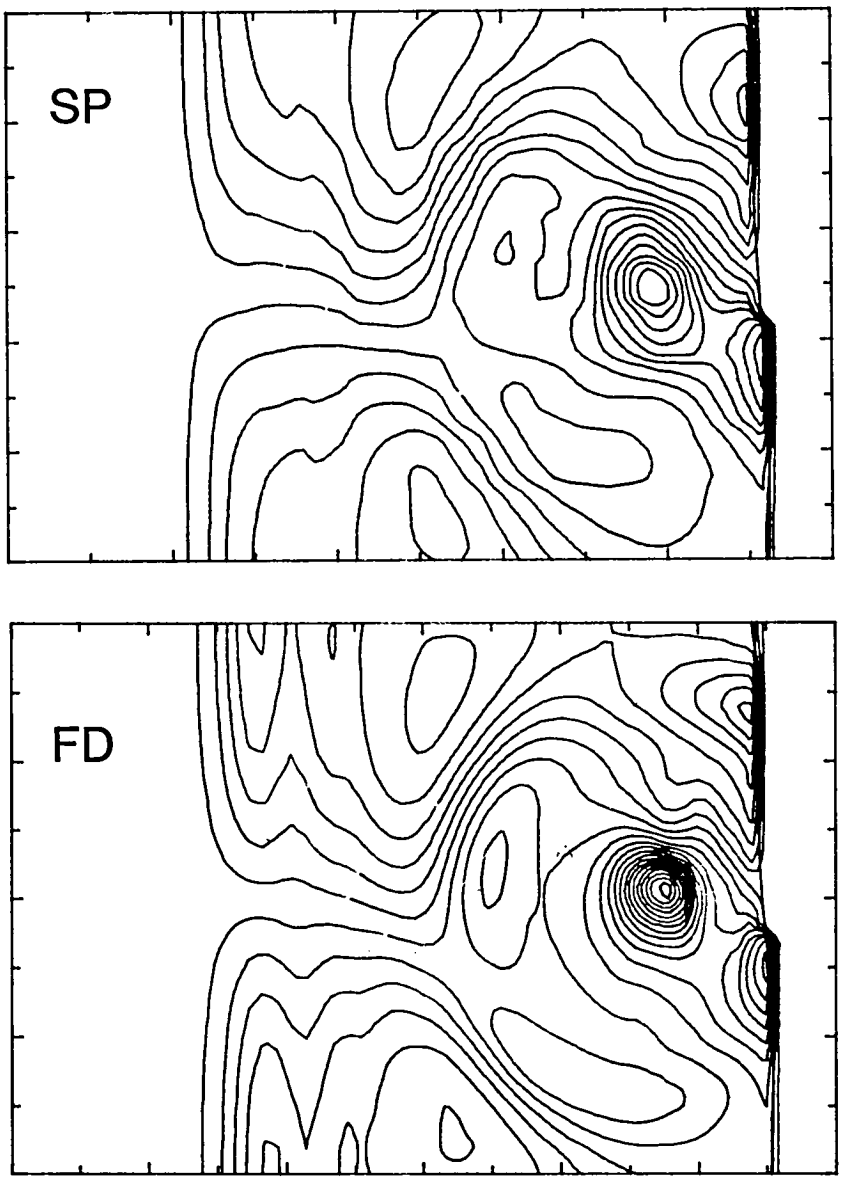

Figure 5

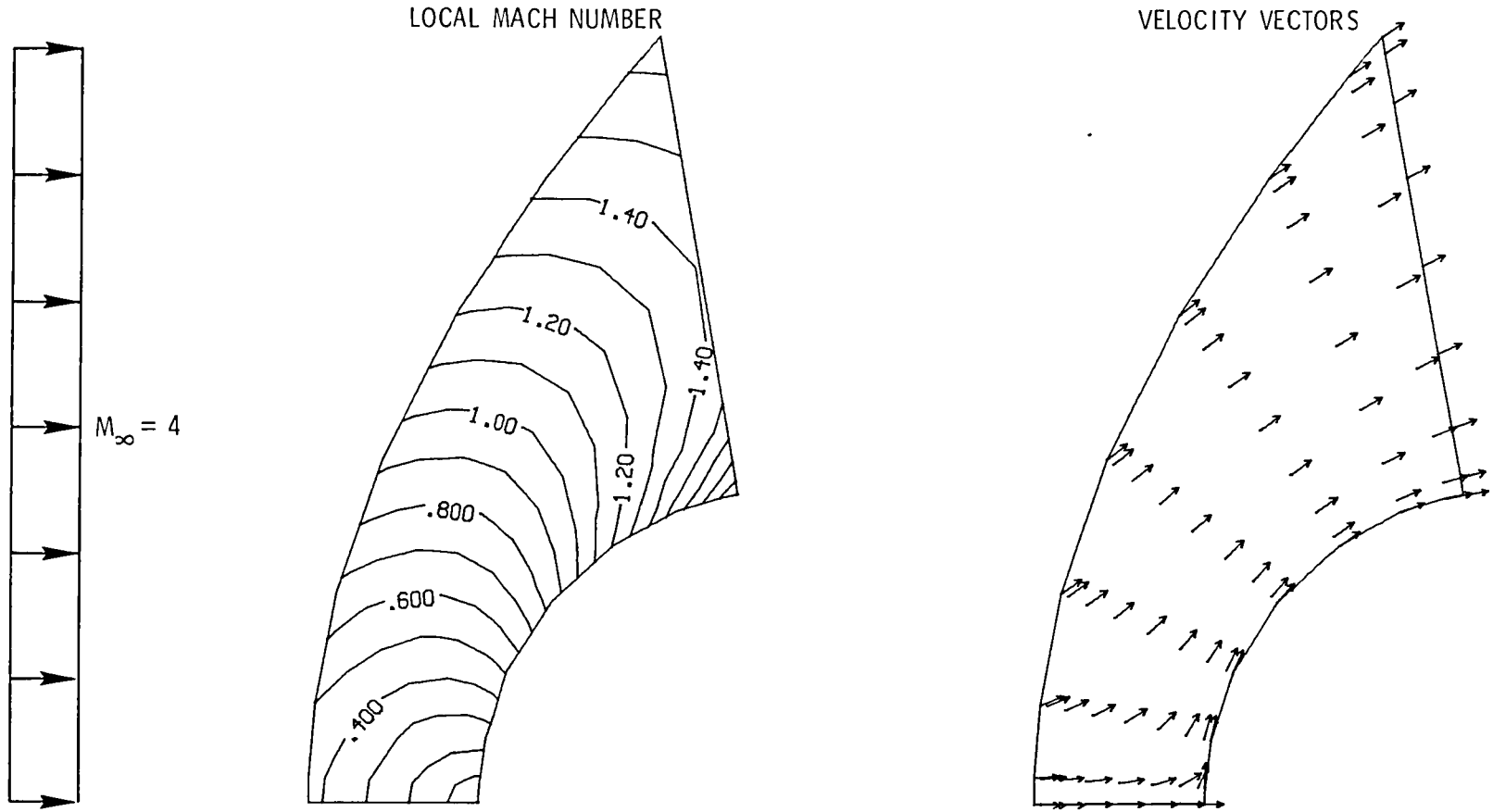
$M_\infty = 4$
LOCAL MACH NUMBER
1.40
1.20
1.00
.800
.600
.400
1.20
1.40
VELOCITY VECTORS

Figure 6

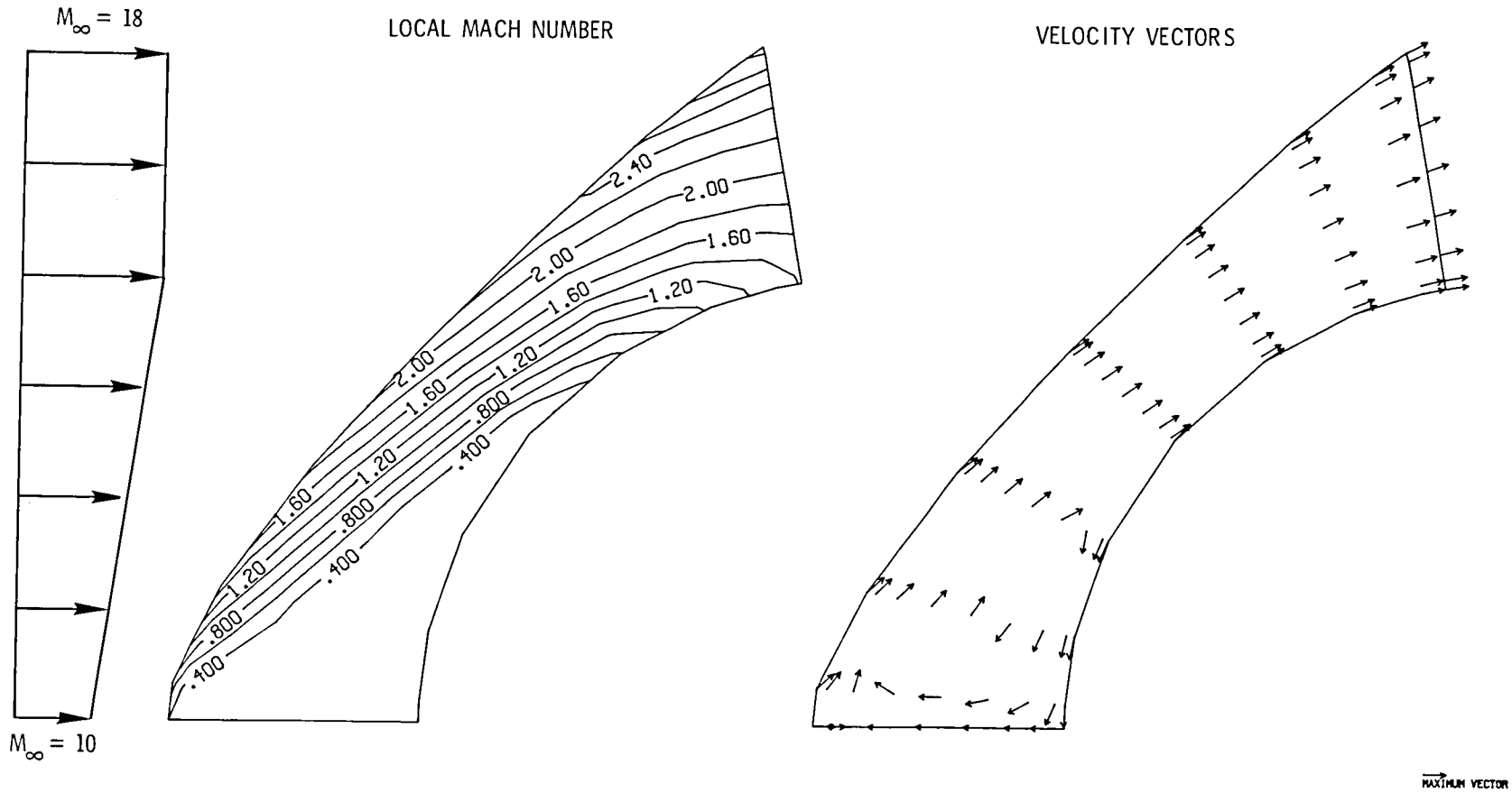
M_∞ = 18
LOCAL MACH NUMBER
VELOCITY VECTORS
2.40
2.00
1.60
1.20
.800
.400
M_∞ = 10
MAXIMUM VECTOR

Figure 7

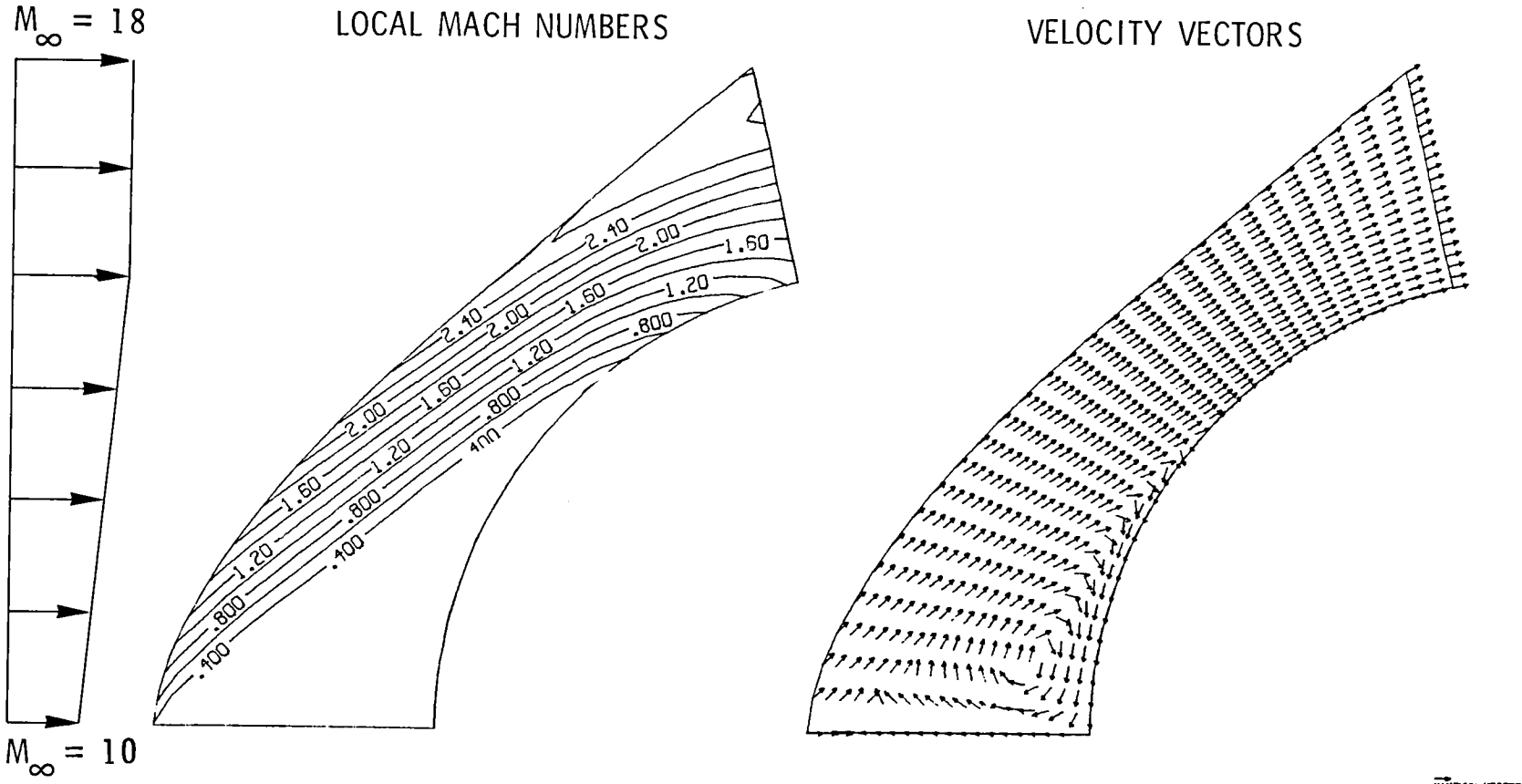
M_∞ = 18
LOCAL MACH NUMBERS
VELOCITY VECTORS
2.40
2.00
1.60
1.20
.800
.400
M_∞ = 10
MAXIMUM VECTOR

Figure 8

1. Report No.	2. Government Accession No.	3. Recipient's Catalog No.
NASA CR-172295		

4. Title and Subtitle	5. Report Date
Spectral Methods for the Euler Equations: Chebyshev Methods and Shock-Fitting	January 1984
	6. Performing Organization Code

7. Author(s)	8. Performing Organization Report No.
M. Y. Hussaini, D. A. Kopriva, M. D. Salas, T. A. Zang	84-4
	10. Work Unit No.

9. Performing Organization Name and Address	11. Contract or Grant No.
Institute for Computer Applications in Science and Engineering Mail Stop 132C, NASA Langley Research Center Hampton, Va 23665	NAS1-17070, NAS1-17130
	13. Type of Report and Period Covered
12. Sponsoring Agency Name and Address	contractor report
National Aeronautics and Space Administration Washington, D.C. 20546	14. Sponsoring Agency Code

15. Supplementary Notes

Langley Techincal Monitor: Robert H. Tolson
Final Report

16. Abstract

The Chebyshev spectral collocation method for the Euler gas-dynamic equations is described. It is used with shock fitting to compute several two-dimensional gas-dynamic flows. Examples include a shock/acoustic wave interaction, a shock/vortex interaction, and the classical blunt body problem. With shock fitting, the spectral method has a clear advantage over second order finite differences in that equivalent accuracy can be obtained with far fewer grid points.

17. Key Words (Suggested by Author(s))	18. Distribution Statement
shock-fitted spectral solutions Euler equations	01 Aeronautics 64 Numerical Analysis Unclassified-Unlimited

19. Security Classif. (of this report)	20. Security Classif. (of this page)	21. No. of Pages	22. Price
Unclassified	Unclassified	35	A03

For sale by the National Technical Information Service, Springfield, Virginia 22161

NASA-Langley, 1984